Phonon-assisted tunneling of electrons in a quantum well/quantum dot injection structure

Adam Mielnik-Pyszczorski, Krzysztof Gawarecki,* and Paweł Machnikowski
Department of Theoretical Physics, Wrocław University of Technology, 50-370 Wrocław, Poland
(Received 29 May 2014; revised manuscript received 23 April 2015; published 18 May 2015)

We study theoretically phonon-assisted relaxation and tunneling in a system composed of a quantum dot which is coupled to a quantum well. Within the $\boldsymbol{k}\cdot\boldsymbol{p}$ method combined with the Löwdin elimination, we calculate the electron states. We calculate acoustic phonon-assisted relaxation rates between the states in the quantum well and in the quantum dot and study the resulting electron kinetics. We show that transition efficiency crucially depends on the system geometry. We show also that under some conditions, transition efficiency can decrease with the temperature.

DOI: 10.1103/PhysRevB.91.195421 PACS number(s): 73.21.La, 73.63.Kv, 63.20.kd

I. INTRODUCTION

Quantum dots (QDs) have been proposed for realization of various optical devices. In particular, QD lasers exhibit many advantages such as low threshold current [1–4], wide spectral tunability [5,6], or high-temperature insensitivity [4,5,7–10]. However, a problem related to the concept of a QD laser is low carrier density inside the dot, which leads to low efficiency [11]. In order to avoid this problem, tunnel injection structures have been developed [12]. Due to high density of states, quantum wells (QWs) are good reservoirs providing carrier supplies for QDs. In a properly designed coupled QW-QD system, carriers can be injected with high speed [11], which considerably increases the optical efficiency. Carrier spectra as well as tunnel coupling have been widely investigated in double quantum dot systems [13–18]. However, the energy structure in QW-QD system differs significantly from that case, due to the existence of the quasicontinuum of states in the QW. Recently, carrier states in such structures have been calculated within eight-band $\boldsymbol{k}\cdot\boldsymbol{p}$ model on a three-dimensional (3D) mesh under periodic boundary condition [19].

The carrier kinetics in the QW-QD systems is also strongly affected by phonon-assisted processes which appear in a crystal environment. Carrier-phonon interaction leads to relaxation between states, which can involve carrier transfer (phonon-assisted tunneling) between the two structures, that is, carrier capture to the QD. The essential role of phonons in the QW-QD injection process is confirmed by experiments [19–24], which indicate that the magnitude of the relaxation rate highly increases when the energy difference between the states of the QD and the QW becomes comparable with the energy of longitudinal optical (LO) phonons. Theoretically, carrier capture between structures of different dimensionality was studied for various systems and on different levels (Fermi golden rule [25], Boltzmann kinetics [26], Green function formalism [27], and full quantum kinetics [28–30]) involving LO phonons [25,26,31] (also including two-phonon effects [31,32]) and Coulomb dynamics [26]. The capture process involving tunneling between a QW and a QD was analyzed within a model including LO phonons and Auger effects, based on a relatively simple model of wave functions [33,34]. On the other hand, it was shown that the exact shape of wave functions may be important for the correct calculation of the capture rates [35]. The carrier dynamics in tunnel injection structures is often limited by the transitions in a conduction band hence it is the conduction band dynamics that attracts much attention both in the theory and in interpreting experiments [23,34]. Efficient hole transfer, in spite of its stronger localization, can be attributed to a great number of valence band states in QD which can provide efficient channels of hole injection [22].

In this work, we study theoretically phonon-assisted tunneling of electrons between a QW and a QD. In order to provide reliable carrier wave functions, which is essential for the study of phonon-assisted tunneling kinetics, and to include the effects of strain in the inhomogeneous system, we base our discussion on wave functions obtained by the $\boldsymbol{k}\cdot\boldsymbol{p}$ method. The carrier kinetics in the system of coupled nanostructures of different dimensionality, induced by the electron coupling to acoustic phonons, is described by equations derived within the correlation expansion framework, which allows us to take into account the quasiequilibrium carrier distribution in the QW and the Pauli blocking effects on the QD state.

The paper is organized as follows. In Sec. II, we present the model. In Sec. III, we discuss the results of the obtained electron states and carrier kinetics. Finally, concluding remarks and discussion are contained in Sec. IV.

II. MODEL

We investigate a vertically stacked system composed of a QW and a QD. The schematic picture of the system under consideration is shown in Fig. 1. We assume homogeneous alloying $In_{0.65}Ga_{0.35}As$ inside the dot, $In_{0.2}Ga_{0.8}As$ in the QW, and $In_{0.41}Ga_{0.59}As$ in the WL. The QW-layer thickness is set to $H_W = 20$ nm, the WL to $H_{WL} = 0.6$ nm, and the QD height to $H_D = 4$ nm and radius $r = 10$ nm (see Fig. 1 for the definition of the geometrical parameters). We assume also an axial symmetry of the system and perform the calculations in cylindrical coordinates (ρ,ϕ,z). Numerical computations are performed in a cylinder with the radius $R_c = 300$ nm and height $H_c = 80$ nm. The results have been verified for convergence with respect to the radius R_c.

The system is strained due to the lattice mismatch between InAs and GaAs. In order to calculate the elements of the strain tensor $\hat{\epsilon}$, we minimized the elastic energy of the system [36,37] in the continuous elasticity approach. Because of the axial

*Krzysztof.Gawarecki@pwr.edu.pl

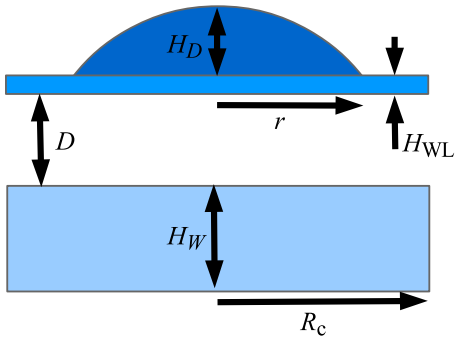

FIG. 1. (Color online) The schematic cross section of the system.

symmetry of the system, the wave functions can be represented in the form

$$\psi_n(\rho,z,\phi) = \frac{1}{\sqrt{2\pi}}\varphi_n(\rho,z)e^{iM\phi},$$

where M is the axial projection of the envelope angular momentum. The local band structure is derived from the eight-band Hamiltonian with strain-induced terms (Bir-Pikus Hamiltonian) using the Löwdin elimination [38,39]. As a result, we obtain the effective Hamiltonian in the form

$$H_c = -\frac{1}{\rho}\frac{\partial}{\partial\rho}\rho\frac{\hbar^2}{2m_\perp(\rho,z)}\frac{\partial}{\partial\rho} - \frac{\partial}{\partial z}\frac{\hbar^2}{2m_z(\rho,z)}\frac{\partial}{\partial z} + \frac{\hbar^2M^2}{2m_\perp(\rho,z)\rho^2} + E_c(\rho,z), \quad (1)$$

with the conduction band edge

$$E_c(\rho,z) = E_{c0} + a_c\mathrm{Tr}\{\hat{\epsilon}\},$$

where E_{c0} is the unstrained bulk conduction band edge. The in-plane component of the effective mass tensor takes the form

$$m_\perp^{-1}(\rho,z) = m_0^{-1}\left(1 + \frac{E_P}{2E_{hh}} + \frac{E_P}{6E_{lh}} + \frac{E_P}{3E_{so}}\right)$$

and the z component of the effective mass is

$$m_z^{-1}(\rho,z) = m_0^{-1}\left(1 + \frac{2E_P}{3E_{lh}} + \frac{E_P}{3E_{so}}\right),$$

where E_P is given by $2m_0P^2/\hbar^2$ (where P is a parameter proportional to the interband matrix transition element), E_g is the energy gap, and energy differences dependent on the position are defined as

$$E_{hh} = E_g + (a_c - a_v)\mathrm{Tr}\{\hat{\epsilon}\} + b_v[\epsilon_{zz} - 0.5(\epsilon_{\rho\rho} + \epsilon_{\phi\phi})],$$
$$E_{lh} = E_g + (a_c - a_v)\mathrm{Tr}\{\hat{\epsilon}\} - b_v[\epsilon_{zz} - 0.5(\epsilon_{\rho\rho} + \epsilon_{\phi\phi})],$$
$$E_{so} = E_g + (a_c - a_v)\mathrm{Tr}\{\hat{\epsilon}\} + \Delta,$$

Δ is the spin-orbit split-off element, a_c,a_v,b_v are the conduction and valence band deformation potentials. The occupations of the electron states in the QW are given by the Fermi-Dirac distribution with the chemical potential μ, which is related to the surface density of the electrons. For a given chemical potential we calculate the concentration of electrons n_e as a sum over all the occupations in the QW divided by the cylinder base surface (πR_c^2). The values of material parameters are the same as in Ref. [18] (following Refs. [40,41]) except for E_p which are 28.0 eV for GaAs and 22.2 eV for InAs.

The Hamiltonian of the system interacting with acoustic phonons is [42]

$$H = \sum_n \epsilon_n a_n^\dagger a_n + \sum_{\boldsymbol{k}\lambda}\hbar\omega_{\boldsymbol{k}\lambda}b_{\boldsymbol{k}\lambda}^\dagger b_{\boldsymbol{k}\lambda} + \sum_{n,m,\boldsymbol{k}\lambda} F_{nm\lambda}(\boldsymbol{k})(b_{\boldsymbol{k}\lambda} + b_{-\boldsymbol{k}\lambda}^\dagger)a_n^\dagger a_m,$$

where ϵ_n denotes the energy of the nth state, $a_{n\lambda}^\dagger$,$a_{n\lambda}$ are the creation and annihilation operators for the electron nth state, respectively, $b_{\boldsymbol{k}\lambda}^\dagger$,$b_{\boldsymbol{k}\lambda}$ are operators of creation and annihilation of a phonon with the wave vector $\boldsymbol{k}$ and phonon branch λ. $F_{nm\lambda}(\boldsymbol{k}) = F_{nm\lambda}^*(-\boldsymbol{k})$ is the electron-phonon coupling constant [42,43]

$$F_{nm\lambda}(\boldsymbol{k}) = \sum_\alpha \mathcal{F}_{nm}(\boldsymbol{k})v_{\boldsymbol{k},\lambda}^{(\alpha)},$$

where $\alpha =$ DP, PE denote the deformation potential and piezoelectric coupling channel. A form factor depending on the wave-function geometry is

$$\mathcal{F}_{nm}(\boldsymbol{k}) = \int_{-\infty}^{\infty} d^3\boldsymbol{r}\,\psi_n^*(\boldsymbol{r})e^{i\boldsymbol{k}\boldsymbol{r}}\psi_m(\boldsymbol{r})$$

and $v_{\boldsymbol{k},\lambda}^{(\alpha)}$ is a material factor

$$v_{\boldsymbol{k}}^{(\mathrm{DP})} = \sqrt{\frac{\hbar k}{2\varrho V c_l}}a_c,$$

$$v_{\boldsymbol{k},\lambda}^{(\mathrm{PE})} = -i\sqrt{\frac{\hbar}{2\varrho V c_\lambda k}}\frac{d_p e}{\epsilon_0\epsilon_r}M_\lambda(\boldsymbol{k}),$$

where $M_\lambda(\boldsymbol{k})$ is a geometrical factor, V is volume of the system, ϱ is a crystal density, d_p is a piezoelectric constant, e is an electron charge, c_λ is speed of sound, $\lambda = \mathrm{s},\mathrm{t}_1,\mathrm{t}_2$ denotes longitudinal and two transversal phonon branches, respectively. The geometrical factor for the zinc-blende structure is

$$M_\lambda(\boldsymbol{k}) = 2[\hat{k}_x(\hat{e}_{\lambda,\boldsymbol{k}})_y\hat{k}_z + \hat{k}_y(\hat{e}_{\lambda,\boldsymbol{k}})_z\hat{k}_x + \hat{k}_z(\hat{e}_{\lambda,\boldsymbol{k}})_x\hat{k}_y],$$

where $\hat{\boldsymbol{k}} = \boldsymbol{k}/k$ and $\hat{e}_{\lambda,\boldsymbol{k}}$ is unit polarization vector of a phonon from the branch λ and with the wave vector $\boldsymbol{k}$. The geometrical factor does not depend on the length of $\boldsymbol{k}$, but only on its direction, so $M_\lambda(\boldsymbol{k}) = M_\lambda(\theta,\phi)$ where

$$\hat{e}_{\mathrm{l},\boldsymbol{k}} \equiv \hat{\boldsymbol{k}} = (\sin\theta\cos\phi, \sin\theta\sin\phi, \cos\theta),$$
$$\hat{e}_{\mathrm{t}1,\boldsymbol{k}} = (-\sin\phi, \cos\phi, 0),$$
$$\hat{e}_{\mathrm{t}2,\boldsymbol{k}} = (\cos\theta\cos\phi, \cos\theta\sin\phi, -\sin\theta).$$

We find the kinetics of the electrons by solving the Heisenberg equation of motion

$$\frac{d}{dt}\langle a_i^\dagger a_i\rangle = \frac{i}{\hbar}\langle[H, a_i^\dagger a_i]\rangle,$$

where $\langle a_i^\dagger a_i\rangle \equiv f_i$ is the average occupation of the ith state. We perform calculations following the correlation expansion (CE) approach. The detailed derivation is given in Appendix B.

As a result, we obtain

$$\dot{f}_i = \sum_{j,\epsilon_j>\epsilon_i} \gamma_{ij}\{f_j[n_B(\omega_{ji})+1] - f_i n_B(\omega_{ji}) - f_i f_j\} + \sum_{j,\epsilon_j<\epsilon_i} \gamma_{ij}\{f_j n_B(\omega_{ij}) - f_i[n_B(\omega_{ij})+1] + f_i f_j\}, \quad (2)$$

where $\omega_{ij} = (\epsilon_i - \epsilon_j)/\hbar$ and γ_{ij} is phonon-assisted relaxation rate given by

$$\gamma_{ij} = 2\pi J_{ij}(\omega_{ji}),$$

where $J_{ij}(\omega_{ji})$ is a phonon spectral density

$$J_{ij}(\omega_{ji}) = \frac{1}{\hbar^2}\sum_{\mathbf{k}\lambda} |F_{ij\lambda}(\mathbf{k})|^2[\delta(\omega_{ji} - \omega_{\mathbf{k}\lambda}) + \delta(\omega_{ji} + \omega_{\mathbf{k}\lambda})],$$

and n_B is the Bose distribution. We took into account coupling to phonons by deformation potential (DP) as well as by piezoelectric field (PE). In order to account how fast charge is flowing into the dot from the QW, we introduce the capture rate as $\gamma_0 = \sum_i \gamma_{0i} f_i[n_B(\omega_{i0})+1]$ where we add all relaxation rates from the states in the QW to the ground state (localized in the QD). This procedure describes phonon-assisted relaxation properly if the state in the QD state is completely unoccupied. Otherwise, the Pauli blockade reduces the charge transfer. In consequence, in order to study the time evolution of the occupations, we numerically solve Eq. (2).

The average number of electrons in the QD was found by $\langle N_{qd}\rangle = \sum_i f_i \eta_i$, where η_i is the probability of finding electron in the ith state in the upper half of the system. The details related with calculations are given in Appendix B.

III. RESULTS

We calculated single-electron states in the considered structure. First, we investigated the influence of strain on electron states. We compared the probability density for the two lowest electron states in a hypothetical structure without strain [Figs. 2(a) and 2(b)] and in a real strained structure [Figs. 2(c) and 2(d)]. In the former case, in order to have similar energy structure as the realistic one, we took a bulk effective mass and we adjusted the conduction band edges to fixed values, constant within each structure (QD, QW, barrier). Ground states in both cases are localized in the QD and their character is the same. As shown in the Fig. 2(b), if the strain field is disabled, the probability density of the lowest state in the QW (which has $M = 0$) has a maximum at $\rho = 0$. In the presence of strain [Fig. 2(d)], the character of this state is different and the density forms a ring. This effect is caused by a repulsive potential generated by the strain field from the QD. However, for higher states in the QW (not shown here) this effect vanishes and for the fourth ($M = 0$) state is no longer clearly visible. The detailed discussion of strain-induced potential generated by the QD is given in Appendix A. Aside from the strain field, carriers could also be affected by a piezoelectric field (and other atomic effects) which lowers the symmetry of the system to C_{2v} and creates two confinement centers in the QW [44].

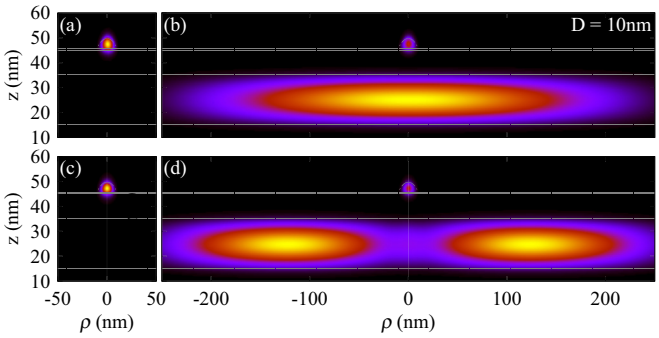

FIG. 2. (Color online) The probability density for the ground state and the first excited state (the lowest state in the QW) in the case of neglected strain field (a), (b) and in the presence of strain field (c), (d).

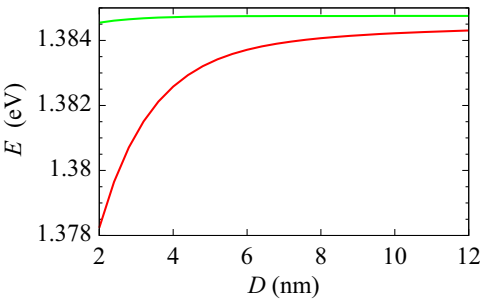

FIG. 3. (Color online) The energies of two lowest states in the system as a function of the distance between the dot and the well.

Figure 3 presents the dependence of the two lowest electron energy levels on the distance D. The ground state is (mainly) localized in the dot and the first excited state is localized in the well. For a small distance, there is a strong tunnel coupling which leads to the large splitting between the energy of states in the QD and in the QW.

Next, we investigated the dependence of the capture rate γ_0 on the distance D. The results are shown in Fig. 4(a). The dependence is nonmonotonic. On the one hand, for closely spaced structures the wave-function overlap between the state localized in the QD and those from the QW is large, which is required for an efficient phonon-assisted relaxation process. On the other hand, strong coupling leads to the large energy splitting, while the phonon spectral density at high frequencies

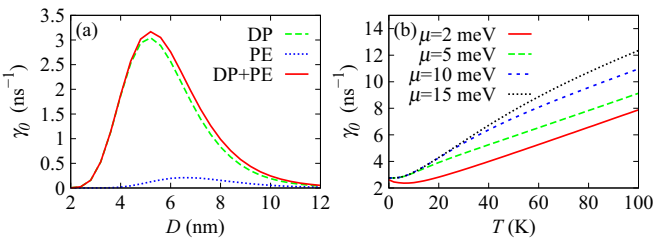

FIG. 4. (Color online) (a) The capture rate at $T = 0$ K and $\mu = 15$ meV ($n_e = 1.5 \times 10^{11}$ cm^{-2}) as a function of the distance between the dot and the well (red solid line) and the contributions to the capture rate due to the DP coupling (green dashed line) and due to the PE coupling (blue dotted line). (b) Temperature dependence of the phonon-assisted relaxation rate at $D = 6$ nm as a function of the temperature.

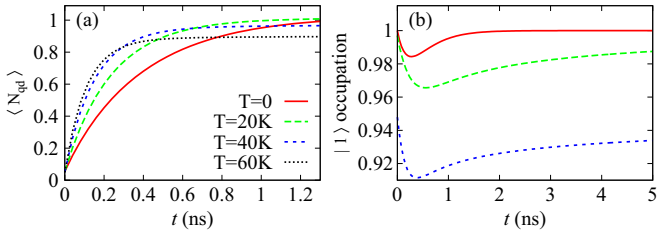

FIG. 5. (Color online) (a) The time evolution of the average number of electrons in the QD at $D = 6$ nm and $\mu = 10$ meV. (b) The time evolution of the lowest QW state occupation.

is low [45,46]. Therefore, the efficiency of relaxation drops down. At large distances, the wave functions for the initial and final states have very small overlap, hence relaxation is also suppressed. The contribution to the capture rate due to the DP coupling is much larger than the one resulting from the PE coupling. The first one has a maximum near $D =$ 5.2 nm, whereas the second one at about 6.6 nm. Similarly as in the double quantum dot case, this shift is related to different spectral densities of the DP and PE reservoirs [37,46]. The PE channel is more efficient at lower frequencies, that is, smaller energy differences between the two states, which corresponds to larger separation between the dots.

We studied also the temperature dependence of the capture rate. In Fig. 4(b), the temperature dependencies for several values of the chemical potential (corresponding to $n_e = 1.9 \times 10^{10}$ to 1.5×10^{11} cm^{-2}) are shown. The observed dependence is linear at high temperatures because, in this case, the leading term of the Bose distribution and Fermi-Dirac distribution is linear ($\sim kT$). The nonzero temperature on the one hand strongly increases the phonon spectral density but also reduces the occupations of electron states below the chemical potential (note that the lowest states in the QW give the predominant contribution in the relaxation process). The latter effect is particularly important at small values of the chemical potential, as shown in Fig. 4(b): for $\mu = 2$ meV ($n_e = 1.9 \times 10^{10}$ cm^{-2}) the relaxation rate decreases with the temperature (for small values of temperature).

We solved Eq. (2) numerically and obtained the electron kinetics. In Fig. 5(a), the time evolution of the average number of electrons in the QD, $\langle N_{qd} \rangle$, is shown at $D = 6$ nm and $\mu = 10$ meV ($n_e = 1.0 \times 10^{11}$ cm^{-2}). As the initial condition, we assume the zero occupation of the ground state (mainly localized in the dot) and Fermi-Dirac distribution in the well. Because of coupling between the dot and the well, the QW states are also partly localized in the dot and at $t = 0$, the occupation of the QD is about 5%. During the time evolution, electrons from the well tunnel into the dot. The time dependence of N_{qd} is nearly exponential with the initial slope similar to γ_0 (but slightly reduced due to the initial occupation). In our simulation, we consider only one spin orientation, hence, the occupation of any orbital state cannot exceed 1, which is assured by the Pauli blocking terms in our kinetic equation. Although there is only one QD state in the energy range accessible for electrons at the temperatures considered here, the occupation of the QD (understood as a relevant volume in space) can slightly exceed 1 due to the tails of the occupied quantum well states that enter the QD region (see, e.g., the green line, $T = 20$ K, in Fig. 5(a)). Increasing the temperature, on the one hand enhances tunneling to the dot, but also enhances the opposite effect (electrons can jump from the dot to the well). At high temperatures, the occupation of the dot is reduced because of the thermal redistribution of occupations from the QD to the QW and also due to decreased occupation of the lowest QW states. Figure 5(b) shows the occupation of the lowest state in the QW. At $T = 0$, the initial occupation is 1, at the beginning of the evolution its value is decreasing because of phonon-assisted tunneling to the dot. However, this effect is small and does not destroy the exponential character of N_{qd} evolution. At later times, higher states from the well also relax and full occupation is restored. In the case of nonzero temperature, the initial occupation is lowered and electron can be excited to the higher state in the QW. In consequence, the initial occupation is no longer recovered. We note also that other relaxation channels (LO phonon coupling or Coulomb scattering) might lead to faster relaxation inside the well [33,34].

IV. CONCLUSIONS

We calculated the electron states in the system of a QD coupled with a QW. We have shown that a strain-dependent repulsive potential repels states in the QW from the dot axis. We investigated the phonon-assisted tunneling and relaxation. We obtained nonmonotonic dependence of the relaxation rate on the distance between the QW and the QD. We studied the temperature dependence of the phonon transitions and we have shown that the value of the capture rate can decrease with temperature. Furthermore, we also investigated the electron kinetics. We obtained the exponential evolution of the average number of electrons in the dot. We also found a nonexponential evolution of the state occupations in the well.

ACKNOWLEDGMENT

This work was supported in parts by the Foundation for Polish Science under the TEAM programme, co-financed by the European Regional Development Fund and by the Grant No. 2012/05/N/ST3/03079 from the Polish National Science Centre (Narodowe Centrum Nauki).

APPENDIX A: STRAIN-INDUCED POTENTIAL IN A QUANTUM WELL

In general, the character of the strain-dependent potential which is generated by the QD in the QW region is related to the ratio between the tensile and compressive strains [44]. If a tensile strain dominates ($\epsilon_{\rho\rho} + \epsilon_{\phi\phi} > \epsilon_{zz}$), the potential is attractive [44]. The attractive harmoniclike potential in a QW was observed experimentally [47,48] and explained in theoretical works [44,49]. However, in the case of a QD considered here (which is close to the "buried dot" case in Ref. [44]), compressive strain in the growth direction (related to ϵ_{zz}) dominates over that related to dilation and the resulting potential on the top of the QW is repulsive.

In order to reproduce the situation of attractive potential we performed additional simulations. We calculated $a_c \mathrm{Tr}\{\hat{\epsilon}\}$, where $\hat{\epsilon}$ is the strain tensor in the QD-QW system. In the case

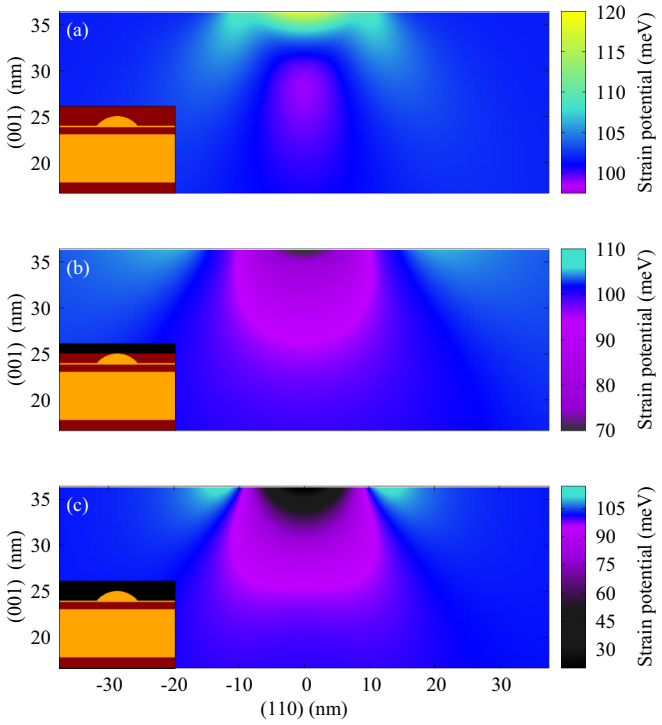

FIG. 6. (Color online) The strain-induced potential inside the QW in the QW-QD system for (a) a QD deeply buried in the GaAs, (b) a QD covered only up to its top, (c) a QD on the surface (uncovered). In sets in bottom left corners are schematic cross sections of the system.

of surface QD, the strain field is relaxed due to expansion of the dot to the top. To model this situation, we introduced a hypothetical very soft material (apart from GaAs and InGaAs) the elastic constants of which (C_{11},C_{12},C_{44}) are 1000 times smaller than those for GaAs and the lattice constant is set to be equal to the GaAs one. Then, the elastic energy of the system is minimized.

We performed the simulation for the geometry and material parameters shown in Sec. II and took the distance $D = 3$ nm. Calculations in this section have been performed on the Cartesian mesh. The strain-induced potential in the QW (below the QD) for the usual situation (that is, a "buried" dot) has been shown in the Fig. 6(a). Because the compressive strain dominates, the potential is mainly repulsive (with attraction in the middle of the QW). Figure 6(b) corresponds to the situation where the QD is buried in a shallow barrier (as shown in the scheme in the corner, GaAs is deposited up to the top of the QD). In that case, the compressive strain in the z direction is reduced compared to the previous situation. In consequence, tensile strain is dominating and the potential becomes attractive. The last situation [Fig. 6(c)] corresponds to the QD on the surface. In this case, the compressive strain is highly reduced and the attractive potential generated in the QW becomes strong.

APPENDIX B: CALCULATION DETAILS

In order to model the evolution of the electron occupations $f_i(t)$, we perform calculation within the CE approach. From the Heisenberg equation for $\langle a_i^\dagger a_j\rangle$ we obtain

$$-i\hbar\frac{d}{dt}\langle a_i^\dagger a_j\rangle = (\epsilon_i-\epsilon_j)\langle a_i^\dagger a_j\rangle + \sum_{n,\boldsymbol{k}\lambda} F_{ni\lambda}(\boldsymbol{k})(\langle a_n^\dagger a_j b_{\boldsymbol{k}\lambda}\rangle + \langle a_n^\dagger a_j b_{-\boldsymbol{k}\lambda}^\dagger\rangle) - \sum_{n,\boldsymbol{k}\lambda} F_{nj\lambda}^*(\boldsymbol{k})(\langle a_n^\dagger a_i b_{\boldsymbol{k}\lambda}\rangle^* + \langle a_n^\dagger a_i b_{-\boldsymbol{k}\lambda}^\dagger\rangle^*).$$

In a similar way, we calculate $\langle a_n^\dagger a_i b_{\boldsymbol{k}\lambda}\rangle$. Here, we assume fast relaxation of the reservoir which allows us to approximate $\langle a_i^\dagger a_j b_{\boldsymbol{k}'\lambda}^\dagger b_{\boldsymbol{k}'\lambda}\rangle \approx \langle a_i^\dagger a_j\rangle\langle b_{\boldsymbol{k}'\lambda}^\dagger b_{\boldsymbol{k}'\lambda}\rangle$. Furthermore, we neglected two-phonon processes $\langle b_{\boldsymbol{k}'\lambda}^\dagger b_{\boldsymbol{k}'\lambda}^\dagger\rangle = \langle b_{\boldsymbol{k}'\lambda} b_{\boldsymbol{k}'\lambda}\rangle = 0$. After all these simplifications, we obtain

$$-i\hbar\frac{d}{dt}\langle a_n^\dagger a_j b_{\boldsymbol{k}\lambda}\rangle = (\epsilon_n-\epsilon_j-\hbar\omega_{\boldsymbol{k}})\langle a_n^\dagger a_j b_{\boldsymbol{k}\lambda}\rangle + \sum_{n'} F_{n'n\lambda}(-\boldsymbol{k})\langle a_{n'}^\dagger a_j\rangle n_B(\omega_{\boldsymbol{k}}) - \sum_{n'} F_{jn'\lambda}(-\boldsymbol{k})\langle a_n^\dagger a_{n'}\rangle[n_B(\omega_{\boldsymbol{k}})+1] + \sum_{n'm} F_{n'm\lambda}(-\boldsymbol{k})\langle a_n^\dagger a_{n'}^\dagger a_j a_m\rangle,$$

where we took $\langle b_{\boldsymbol{k}'\lambda}^\dagger b_{\boldsymbol{k}\lambda}\rangle = n_B(\omega_{\boldsymbol{k}})\delta_{\boldsymbol{k}'\boldsymbol{k}}$. The electron correlations are accounted for within the Hartree-Fock approximation $\langle a_i^\dagger a_n^\dagger a_j a_m\rangle \approx \langle a_i^\dagger a_m\rangle\langle a_n^\dagger a_j\rangle - \langle a_i^\dagger a_j\rangle\langle a_n^\dagger a_m\rangle$. This yields a closed set of equations for $\langle a_i^\dagger a_j\rangle$ and $\langle a_i^\dagger a_j b_{\boldsymbol{k}}\rangle$. The latter is then formally integrated and substituted to the former. Since we describe real transitions which, in our case, are much slower than characteristic times of the memory of phonon-reservoir (tens of ps versus several ps) we perform the Markov approximation. This approach would be insufficient if dephasing of coherences was of interest [50], in particular if evolution in real space was to be traced [30]. These limitations of the Markov approximation can be overcome either by an extended version of the approach presented here [30] or by more exact methods [50,51] which may, however, be limited by the complexity (large number of states) of the present system. Upon performing the Markov and secular approximations, we obtain

$$\dot{f}_i = \sum_{j,\epsilon_j>\epsilon_i}\gamma_{ij}\{f_j[n_B(\omega_{ji})+1] - f_i n_B(\omega_{ji}) - f_i f_j\} + \sum_{j,\epsilon_j<\epsilon_i}\gamma_{ij}\{f_j n_B(\omega_{ij}) - f_i[n_B(\omega_{ij})+1] + f_i f_j\}. \quad \text{(B1)}$$

This set of differential equations is solved numerically using the GSL library [52].

The Schrödinger equation with the Hamiltonian given by Eq. (1) is solved numerically on a two-dimensional grid. The eigenproblem has been solved using Lanczos method combined with the shift-invert spectral transformation where the linear set of equations is solved using the LIS library [53].

In order to check the validity of modeling an infinite well in a finite cylinder, we calculated the capture rate γ_0 as a

function of cylinder radius R_c. We confirmed that γ_0 converge at $R_c = 300$ nm. The reason for this convergence in spite of the quantized spectrum in the cylinder (as opposed to the actual continuum restored in the limit $R_c \to \infty$) is as follows: when the radius of the cylinder increases, the overlap between the wave function in the QD and those localized in the QW decreases like $\sim 1/R_c^2$. On the other hand, with increasing cylinder size, the density of QW states increases as $\sim R_c^2$. As a result, for a sufficiently large cylinder, convergence is reached.

[1] G. T. Liu, A. Stintz, H. Li, K. Malloy, and L. Lester, Electron. Lett. **35**, 1163 (1999).

[2] M. Asada, Y. Miyamoto, and Y. Suematsu, IEEE J. Quantum Electron. **22**, 1915 (1986).

[3] O. Shchekin and D. Deppe, IEEE Photon. Technol. Lett. **14**, 1231 (2002).

[4] O. Shchekin, J. Ahn, and D. Deppe, Electron. Lett. **38**, 712 (2002).

[5] P. Varangis, H. Li, G. T. Liu, T. Newell, A. Stintz, B. Fuchs, K. Malloy, and L. Lester, Electron. Lett. **36**, 1544 (2000).

[6] D. I. Nikitichev, K. A. Fedorova, Y. Ding, A. Alhazime, A. Able, W. Kaenders, I. Krestnikov, D. Livshits, and E. U. Rafailov, Appl. Phys. Lett. **101**, 121107 (2012).

[7] O. B. Shchekin and D. G. Deppe, Appl. Phys. Lett. **80**, 3277 (2002).

[8] N. Kirstaedter, N. N. Ledentsov, M. Grundmann, D. Bimberg, V. M. Ustinov, S. S. Ruvimov, M. V. Maximov, P. S. Kop'ev, Z. I. Alferov, U. Richter, P. Werner, U. Gösele, and J. Heydenreich, Electron. Lett. **30**, 1416 (1994).

[9] S. Fathpour, Z. Mi, P. Bhattacharya, A. R. Kovsh, S. S. Mikhrin, I. L. Krestnikov, A. V. Kozhukhov, and N. N. Ledentsov, Appl. Phys. Lett. **85**, 5164 (2004).

[10] M. Maksimov, N. Gordeev, S. Zaitsev, P. Kop'ev, I. Kochnev, N. Ledentsov, A. Lunev, S. Ruvimov, A. Sakharov, A. Tsatsul'nikov, Y. Shernyakov, Z. Alferov, and D. Bimberg, Semiconductors **31**, 124 (1997).

[11] P. Bhattacharya, S. Ghosh, S. Pradhan, J. Singh, Z.-K. Wu, J. Urayama, K. Kim, and T. Norris, IEEE J. Quantum Electron. **39**, 952 (2003).

[12] Z. Mi, S. Fathpour, and P. Bhattacharya, Electron. Lett. **41**, 1282 (2005).

[13] G. W. Bryant, Phys. Rev. B **47**, 1683 (1993).

[14] M. Bayer, P. Hawrylak, K. Hinzer, S. Fafard, M. Korkusinski, Z. R. Wasilewski, O. Stern, and A. Forchel, Science **291**, 451 (2001).

[15] M. Korkusiński and P. Hawrylak, Phys. Rev. B **63**, 195311 (2001).

[16] A. Schliwa, O. Stier, R. Heitz, M. Grundmann, and D. Bimberg, Phys. Status Solidi B **224**, 405 (2001).

[17] G. Bester, J. Shumway, and A. Zunger, Phys. Rev. Lett. **93**, 047401 (2004).

[18] K. Gawarecki, P. Machnikowski, and T. Kuhn, Phys. Rev. B **90**, 085437 (2014).

[19] M. Syperek, J. Andrzejewski, W. Rudno-Rudziński, G. Sęk, J. Misiewicz, E. M. Pavelescu, C. Gilfert, and J. P. Reithmaier, Phys. Rev. B **85**, 125311 (2012).

[20] E.-M. Pavelescu, C. Gilfert, J. P. Reithmaier, A. Martin-Minguez, and I. Esquivias, IEEE Photon. Technol. Lett. **21**, 999 (2009).

[21] G. Sęk, J. Andrzejewski, K. Ryczko, P. Poloczek, J. Misiewicz, E. S. Semenova, A. Lemaitre, G. Patriarche, and A. Ramdane, Semicond. Sci. Technol. **24**, 085011 (2009).

[22] X.-J. Yang, T. Kiba, T. Yamamura, J. Takayama, A. Subagyo, K. Sueoka, and A. Murayama, Appl. Phys. Lett. **104**, 012406 (2014).

[23] W. Rudno-Rudziński, G. Sęk, K. Ryczko, M. Syperek, J. Misiewicz, E. S. Semenova, A. Lemaitre, and A. Ramdane, Appl. Phys. Lett. **94**, 171906 (2009).

[24] W. Rudno-Rudziński, G. Sęk, K. Ryczko, M. Syperek, J. Misiewicz, E. S. Semenova, A. Lemaitre, and A. Ramdane, Phys. Status Solidi A **206**, 826 (2009).

[25] R. Ferreira and G. Bastard, Appl. Phys. Lett. **74**, 2818 (1999).

[26] T. R. Nielsen, P. Gartner, and F. Jahnke, Phys. Rev. B **69**, 235314 (2004).

[27] J. Seebeck, T. R. Nielsen, P. Gartner, and F. Jahnke, Phys. Rev. B **71**, 125327 (2005).

[28] M. Glanemann, V. M. Axt, and T. Kuhn, Phys. Rev. B **72**, 045354 (2005).

[29] D. Reiter, M. Glanemann, V. M. Axt, and T. Kuhn, Phys. Rev. B **73**, 125334 (2006).

[30] D. Reiter, M. Glanemann, V. M. Axt, and T. Kuhn, Phys. Rev. B **75**, 205327 (2007).

[31] I. Magnusdottir, A. V. Uskov, S. Bischoff, B. Tromborg, and J. Mørk, J. Appl. Phys. **92**, 5982 (2002).

[32] J.-Z. Zhang and I. Galbraith, Appl. Phys. Lett. **89**, 153119 (2006).

[33] S. L. Chuang and N. Holonyak, Appl. Phys. Lett. **80**, 1270 (2002).

[34] S. W. Chang, S. L. Chuang, and N. Holonyak, Phys. Rev. B **70**, 125312 (2004).

[35] T. Markussen, P. Kristensen, B. Tromborg, T. W. Berg, and J. Mørk, Phys. Rev. B **74**, 195342 (2006).

[36] C. Pryor, J. Kim, L. W. Wang, A. J. Williamson, and A. Zunger, J. Appl. Phys. **83**, 2548 (1998).

[37] K. Gawarecki, M. Pochwała, A. Grodecka-Grad, and P. Machnikowski, Phys. Rev. B **81**, 245312 (2010).

[38] T. B. Bahder, Phys. Rev. B **41**, 11992 (1990).

[39] P. O. Löwdin, J. Chem. Phys. **19**, 1396 (1951).

[40] I. Vurgaftman, J. R. Meyer, and L. R. Ram-Mohan, J. Appl. Phys. **89**, 5815 (2001).

[41] A. Schliwa, M. Winkelnkemper, and D. Bimberg, Phys. Rev. B **76**, 205324 (2007).

[42] A. Grodecka, P. Machnikowski, and J. Förstner, Phys. Rev. B **78**, 085302 (2008).

[43] A. Grodecka, L. Jacak, P. Machnikowski, and K. Roszak, in *Quantum Dots: Research Developments*, edited by P. A. Ling (Nova Science, NY, 2005), p. 47.

[44] J. H. Davies, Appl. Phys. Lett. **75**, 4142 (1999).
[45] K. Gawarecki and P. Machnikowski, Phys. Rev. B **85**, 041305 (2012).
[46] J. Wu and Z. M. Wang, *Quantum Dot Molecules* (Springer, New York, 2014).
[47] H. Lee, J. A. Johnson, J. S. Speck, and P. M. Petroff, J. Vacuum Sci. Technol. B **18**, 2193 (2000).
[48] H. Lipsanen, M. Sopanen, and J. Ahopelto, Phys. Rev. B **51**, 13868 (1995).
[49] J. Tulkki and A. Heinämäki, Phys. Rev. B **52**, 8239 (1995).
[50] M. Glässl, A. Vagov, S. Lüker, D. E. Reiter, M. D. Croitoru, P. Machnikowski, V. M. Axt, and T. Kuhn, Phys. Rev. B **84**, 195311 (2011).
[51] A. Vagov, M. D. Croitoru, M. Glässl, V. M. Axt, and T. Kuhn, Phys. Rev. B **83**, 094303 (2011).
[52] M. Galassi, J. Davies, J. Theiler, B. Gough, G. Jungman, M. Booth, and F. Rossi, Gnu Scientific Library: Reference Manual, 2nd ed., Network Theory Ltd., http://www.gnu.org/software/gsl/
[53] A. Nishida, *Computational Science and Its Applications- ICCSA 2010*, Vol. 6017 of Lecture Notes in Computer Science (Springer, Berlin, 2010), pp. 448–462.